Journal of Thermal Engineering
Web page info: https://jten.yildiz.edu.tr
DOI: 10.18186/thermal.1201859

Research Article

Numerical investigation of heat transfer & hall effects on MHD nanofluid flow past over an oscillating plate with radiation

S. SARALA[1,*], E. GEETHA[2], M. NIRMALA[3]

[1]*Department of Mathematics, AVIT, Vinayaka Missions Research Foundation,Chennai,Tamilnadu, India*
[2]*Department of Mathematics, Sri Chandrasekharendra Saraswathi Viswa Maha Vidyalaya, Tamilnadu, India*
[3]*Department of Mathematics, Kumararani Meena Muthiah College of Arts and Science, Tamilnadu, India*

ARTICLE INFO

Article history
Received: 15 February 2021
Accepted: 29 May 2021

Keywords:
Nanofluid; Oscillating plate; Magnetohydrodynamic; Radiation; Hall Parametery

ABSTRACT

The effects of convective heat generation and the oscillatory motion of a plate in the presence of MHD, Alumina nanofluid fl ow, thermal radiation, and Hall current are co nsidered. The plate oscillates harmonically in its axes with uniform temperature. Th e dimensional equations have to be changed into non-dimensional equations with a set of dimensionless parameters. The Laplace transformation technique is utilized to get an exact solution. The possessions of velocity and temperature are analyzed with several parameters like Prandtl number (Pr), Grashof number (Gr), Hall parameter (m), magnetic parameter (M), radiation (R), solid volume fraction(φ), phase angle(ω).The influence of primary and secondary velocity is discussed by the graph. It is observed that the increment of Hall parameter (m) diminishes the primary velocity, an increment of Grashof number leads to an increase in both velocities, and increasing solid volume fraction raises the temperature. The Nusselt number and skin friction coefficient values have expressed in the table. It is apparent that an increment of radiation increased the value of the Nusselt number and also an increment of phase angle value diminished the skin friction coefficient value.

Cite this article as: Sarala S, Geetha E, Nirmala M. Numerical investigation of heat transfer & hall effects on mhd nanofluid flow past over an oscillating plate with radiation. J Ther Eng 2022;8(6):757–771.

INTRODUCTION

A nanofluid contains colloidal suspensions of a nanometer-sized particle which is rapidly settling in fluid and stay suspended much longer than a microparticle. With the increasing influence of microprocessors and other electronic types of machinery, a pursuit for a more efficient heat-dissipating system has created nowadays an enigmatic career. Nanofluids are playing a major role in heat transfer. New prototypical nanofluids have to consider

***Corresponding author.**
*E-mail address: saralashun@gmail.com, geethamuthu06@gmail.com, nirmalswamy@gmail.com

This paper was recommended for publication in revised form by Regional Editor Tolga Taner

the surface area, size, structure-dependent behavior, and boundary resistance for thermal conductivity. The heat flux is increased by the conventional method. The automobile, electrical, and electronics companies have faced the challenges to reduce the heat level in the prototype of manufacturing. The thermal conductivity increases on the accumulation ofalumina nanofluids to normal fluids. The Alumina particle regulates the pH value in a wide range. It is an eco-friendly particle that is used in water purification and cosmetics production. Oscillating flows characterize a significant feature of conventional fluid dynamics. The oscillating plate is encouraged heat and mass transfer which is attained by fluid shaking around an immovable item or shaking of a solid form in any fluid. The Al_2O_3 nanofluid is acted as a coolant in double tube heat exchangers. It is extensively used in ceramics, nanocomposites, catalyst support, heat transfer fluids, water-resistant additives.

The numerical solution is the stability among the computational period and exactness of the solution. CongTam Nguyen et al. [1] have analyzed 36 nm and 47 nm particle size in a nanofluid. The heat and mass transmission of the vertical plate with MHD was analyzed by Muthucumaraswamy et al. [2]. Veeranna Sridhara et al. [3] reviewed Alumina nanofluid. He collected the experiment results of nanofluids which have substantially higher thermal conductivities than base fluid. The transport andthermal properties of the base fluid are converted by nanoparticles. Bhaskar Chandra Sarkar et al. [4] revealed that unsteady primary flow Hall current leads to a decrease in the amplitude of the shear stress. Lee et al. [5] experimentally inspected the thermal conductivity performance of dilute nanofluids by a transient hot-wire technique. On rotating a porous plate with chemically reactive fluid, impacts of hall current and radiation on MHD convective heat and mass transmission were contemplated by Dual pal et al. [6]. Mohammad Reza Mohaghegh [7] suggested a spectral algorithmfor the fast and competent computation of periodic flows. Siddarth Roy et al. [8]studied the heat transfer characteristics of silver/water nanofluid in a solar flat plate collector. Rajesh et al. [9] related to magnetic nanomaterial thermal flow in engineering branches and identified key development of thermal radiation heat flux in nanomaterial fabrication.

Mohaghegh et al. [10] have used periodic boundary conditions exclusively for oscillation bodies. Das et al. [11] compared Copper, Alumina, and Titania nanofluid flow with Hall effects and radiation in rotating angular velocity. Veera Krishna et al. [12] deliberated Hall effects in the oscillating porous plate with a graph that was drawn using MATHEMATICA software. Dastagiri Babu et al. [13] had instructed to neglect Hall Effect with a very small value of Reynolds number and absence of electric field. He noticed that the velocity value decreases with the increasing intensity of the magnetic parameter (M). Obulesu et al. [14] studied chemical reaction, buoyancy effects of thermal and mass diffusion with Hall effects. He assumed constant heat generation in volumetric. Hussain et al. [15] investigated the effects of Hall current and pointed out that neither energy was added nor deducted from the fluid in the electric field. Gauri Shankar Seth et al. [16]acknowledged fluid temperature and fluid velocity slowdown in ramped temperature plates instead of the isothermal plate. Sebiha Yıldız [17] has discussed the natural cooling process for reducing excess heat. He also investigated various directions at different angles of inclination for cooling a plate. Kataria et al. [18] are concerned about the heat and mass transfer of Casson fluid flow past over an oscillating plate. He analyzed the oscillating plate with ramp temperature and concentration. On the oscillating plate, Vijayalakshmi et al. [19] have explored the unchanging heat and mass flux with radiation, MHD, in presence of the chemical. Iqbal et al. [20] examined the combined reactions of radiation, Hall currents and analyzed different shapes of nanoparticles. Arifuzzaman et al. [21] considered high-speed MHD nanofluid flow with chemical reaction and radiation effect. He optimized numerical values of flow parameters and evaluated momentum and thermal boundary layer thickness. He noticed that the same order of Coriolis and viscous forces magnitude which is called Ekman layer formation near the plate.Siva Reddy et al. [22] compared the numerical values of skin friction and Nusselt number with previously published work and interpret the current values. Radha Madhavi et al. [23] have considered Alumina (Al_2O_3) nanoparticles with water and kerosene as the base fluid. Heat generation has been increased the heat transfer process and motion. Brinkman fluid had been chosen for the experiment by Arshad Khan et al. [24].Patel et al. [25] contemplated the effects of radiation, Hall current in an oscillating plate in a porous medium. He investigated isothermal temperature with the ramped wall temperature of the plate. He talked about MHD applications in various fields. He examined four different kinds of nanoparticles for computational.

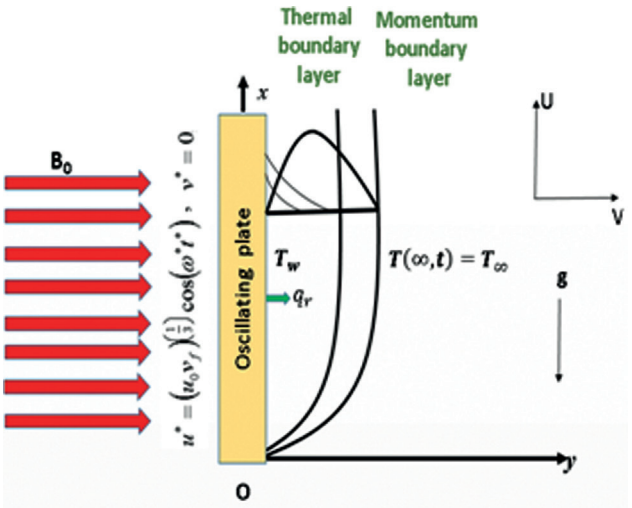

Figure 1. The physical model and coordinate system.

Dharmaiah et.al. [26] have taken Titanium alloy water-based nanofluid and a two-term analytical method applied to get a closed-form solution. Baby rani et al. [27]used Ag-water-based nanofluid and applied perturbation technique to solve nonlinear ordinary differential equations. Manjula et al. [28] carried the Dufour number with thermal radiation and chemical reaction. Balaji et al. [29] examined various cooling methods specifically the liquid cooling method with nanometer-sized particles of nanofluids. From the above literature review, they discussed the effects of particle size, the thickness of boundary layer, various nanofluid flow, different base fluid, heat reduction, MHD, radiation.

The physical model and coordinate system of a problem are shown in Figure 1.A lot of applications from the industry created important attention and motivated by the above literature review. The effects of MHD nanofluid flow of an incompressible viscous fluid past an oscillating vertical plate in the presence of Hall effects and radiation have not been studied in all the above-cited papers. In this paper, alumina-water is used.

To our knowledge, no attempts have been made to study the effects of MHD nanofluid flow of an oscillating vertical plate is considered in the presence of Hall effects and radiation.

MATHEMATICAL ANALYSIS

In the presence of thermal radiation, the viscous flow of an incompressible Al_2O_3 nanofluid past an oscillating vertical plate has been considered. The x^* oy^* the plane is taken and $z^*= 0$. At time $t \le 0$, the plate and fluid are at the same temperature T_∞. The plate has oscillated along the x^* axis and the y^* axis is normal for the remaining axes. Near the plate, the temperature value is expected T_∞. The velocity $u^* = \left(u_0 v_f\right)^{\left(\frac{1}{3}\right)} \cos\left(\omega^* t^*\right)$ is started oscillating and the temperature surges to T_W. The uniform magnetic field B_0 is applied uniformly parallel to the z^* axis. The radiative heat flux q_r is applied in the normal direction to the plate.Thermo-physical properties of water and Alumina nanoparticles are tabulated in Table 1.

The equation of continuity is $\nabla \cdot \vec{F} = 0$ where u^*, v^*, w^* denotes the components of the velocity vector $\vec{F}$. It provides $w^*= 0$ inflow which is satisfied by the plate everywhere. The external velocity varies inversely–linear with the distance along the surface which is known as Pseudo similarity. In this similarity transformation, the velocity similarity variables are taken as the core similarity variables. It is denoted by η. Thewater-based Al_2O_3 nanoparticles are taken as a fluid. The base fluid and the suspended nanoparticles are carried which are in thermal equilibrium.

Z* and t* direct the flow. The flow far away from the plate without disruption is considered.

The unstable flow of usual Boussinesq's approximation governing equations are as follows:

$$\rho_{nf}\frac{\partial u^*}{\partial t^*} = \mu_{nf}\frac{\partial^2 u^*}{\partial z^{*2}} + g(\rho\beta)_{nf}(T - T_\infty) + \frac{\sigma_{nf}B_0^2\left(mv^* - u^*\right)}{\left(1+m^2\right)} \tag{1}$$

$$\rho_{nf}\frac{\partial v^*}{\partial t^*} = \mu_{nf}\frac{\partial^2 v^*}{\partial z^{*2}} - \frac{\sigma_{nf}B_0^2\left(v^* + mu^*\right)}{\left(1+m^2\right)} \tag{2}$$

$$(\rho c_p)_{nf}\frac{\partial T}{\partial t^*} = k_{nf}\frac{\partial^2 T}{\partial z^{*2}} - \frac{\partial q_r}{\partial z^*} \tag{3}$$

where u^* is the primary velocity and v^* is the secondary velocity.

The initial and boundary conditions of the projected problem are given by:

$$\begin{aligned} &u^* = 0, \quad v^* = 0, \quad T = T_\infty \quad for\,all \quad z^*, t^* \le 0 \\ &u^* = \left(u_0 v_f\right)^{\left(\frac{1}{3}\right)} \cos\left(\omega^* t^*\right), \quad v^* = 0, \\ &\qquad\qquad T = T_w \;\; at\, z^* = 0 \;\; for\,all \;\; t^* > 0 \\ &u^* \to 0, \qquad v^* \to 0, \quad T \to T_\infty \quad at \quad z^* \to \infty \end{aligned} \tag{4}$$

On introducing the following non-dimensional quantities are:

$$U = \frac{u^*}{\left(u_0 v_f\right)^{\left(\frac{1}{3}\right)}}, \quad V = \frac{v^*}{\left(u_0 v_f\right)^{\left(\frac{1}{3}\right)}}, \quad Z = z^*\left(\frac{u_0}{v_f^2}\right)^{\left(\frac{1}{3}\right)}$$

$$\omega = \omega^*\left(\frac{v_f}{u_0^2}\right)^{\left(\frac{1}{3}\right)}$$

Table 1. Thermo-physical properties of water and Alumina nanoparticles

Physical Properties	ρ (kg / m^3)	C_p (J/KgK)	K(W / mK)	$\beta \times 10^5$ (K^{-1})	φ	σ(S/m)
Water / Base fluid	997.1	4179	0.613	21	0.0	5.5×10^{-6}
Al_2O_3 (Alumina)	3970	765	40	0.85	0.15	35×10^6

$$\theta = \frac{T - T_\infty}{T_w - T_\infty}$$

$$Gr = \frac{g\,\beta_f (T_w - T_\infty)}{u_0}$$

$$R = \frac{16\,a^*\,\sigma_f T_\infty^{\,3}}{k_f}\left(\frac{\%\rho^2}{u_0}\right)^{\left(\frac{1}{3}\right)}$$

$$\Pr = \frac{\mu c_p}{k_f}$$

$$M^2 = \frac{\sigma_f B_0^2}{\rho_f}\left(\frac{\nu_f}{u_0^{\,2}}\right)^{\left(\frac{1}{3}\right)}$$

The local radiant for the case of an optically thin gray gas is expressed by

$$\frac{\partial q_r}{\partial z^*} = -4a^*\,\sigma_f\left(T_\infty^4 - T^4\right) \tag{5}$$

It is assumed that the temperature differences within the flow are sufficiently small such that T^4 may be expressed as a linear function of the temperature. This is accomplished by expanding T^4 in a Taylor series about T_∞ and neglecting higher-order terms, thus

$$T^4 \cong 4T_\infty^3\,T - 3T_\infty^4 \tag{6}$$

By using equations, dimensionless parameter equation (3) reduces to

$$(\rho c_p)_{nf}\,\frac{\partial T}{\partial t'} = k_{nf}\,\frac{\partial^2 T}{\partial z^{*2}} + 16a^*\sigma T_\infty^3\,(T_\infty - T) \tag{7}$$

By using the dimensionless parameter, equations Eq. (1), Eq. (2), and Eq. (3) leads to,

$$L_1\frac{\partial U}{\partial t} = L_3\frac{\partial^2 U}{\partial Z^2} + L_4\frac{(U - mV)M^2}{1+m^2} + L_2 Gr.\theta \tag{8}$$

$$L_1\frac{\partial V}{\partial t} = L_3\frac{\partial^2 V}{\partial Z^2} - L_4\frac{(mU + V)M^2}{1+m^2} \tag{9}$$

$$L_5\frac{\partial \theta}{\partial t} = L_6\frac{1}{\Pr}\frac{\partial^2 \theta}{\partial Z^2} - \frac{R}{\Pr}\theta \tag{10}$$

Where

$$L_1 = (1-\phi) + \phi\left(\frac{\rho_s}{\rho_f}\right)$$

$$L_2 = (1-\phi) + \phi\left(\frac{(\rho\beta)_s}{(\rho\beta)_f}\right)$$

$$L_3 = \frac{1}{(1-\phi)^{2.5}}$$

$$L_4 = 1 + \frac{3(\sigma-1)\,\phi}{(\sigma+2) - (\sigma-1)\,\phi}, \qquad \sigma = \frac{\sigma_s}{\sigma_f}$$

$$L_5 = (1-\phi) + \phi\left(\frac{(\rho c_p)_s}{(\rho c_p)_f}\right)$$

$$L_6 = \left[\frac{k_s + 2k_f - 2\phi(k_f - k_s)}{k_s + 2k_f + \phi(k_f - k_s)}\right]$$

Where R is the radiation parameter, Pr is the Prandtl number, Gr is the thermal Grashof number, and Gr approximates the ratio of the buoyancy force to the viscous force acting. Large R signifies a large radiation effect while R→0 corresponds to zero radiation effect.

The corresponding initial and boundary conditions are represented by Eq. (11),

$$\begin{gathered} U = 0, \quad V = 0, \quad \theta = 0 \quad for\,all \quad Z, t \le 0 \\ t > 0:\ U = Cos(\omega t), \quad V = 0, \quad \theta = 1 \quad at \quad Z = 0 \\ U \to 0, \qquad V \to 0,\ \theta \to 0 \ \ at \ \ Z \to \infty \end{gathered} \tag{11}$$

$$\text{Let } F = U + iV \tag{12}$$

The newest governing equations are

$$L_1\frac{\partial F}{\partial t} = L_3\frac{\partial^2 F}{\partial Z^2} - L_4\frac{F(1+im)M^2}{1+m^2} + L_2 Gr.\theta \tag{13}$$

$$L_5\frac{\partial \theta}{\partial t} = L_6\frac{1}{\Pr}\frac{\partial^2 \theta}{\partial Z^2} - \frac{R}{\Pr}\theta \tag{14}$$

The newest initial and boundary conditions are,

$$\begin{gathered} F = 0, \qquad \theta = 0 \ \ for\ \ all\ Z, t \le 0 \\ t > 0:\ F = Cos\left(\omega t\right), \qquad \theta = 1 \ \ at \ \ Z = 0 \\ F \to 0, \qquad \theta \to 0 \ \ at \ \ Z \to \infty \end{gathered} \tag{15}$$

SOLUTION PROCEDURE

The solutions are in terms of the exponential and complementary error functions. The relation connecting the

error function and its complementary error function is as follows:

$$erfc(x) = 1 - \mathrm{erf}(x) \tag{16}$$

Rajesh et al. [9] have been solved equations by the implicit finite-difference method of the Crank-Nicolson type. Vijayalakshmi et al. [19] changed partial differential equations into an ordinary differential equation using similarity transformation and applied the Runge-Kutta method to find a solution.

Laplace transformation technique is applied in the development of time-domain fluid line models, signal processing, control systems, statistical mechanics, data mining, and machine learning. Laplace transform deals with unsteady-state difficulties of transport phenomena.The standard Laplace transformation is used to solve the major dimensionless equations Eq. (13) and Eq. (14) along with conditional equations Eq. (15).The results are explained as follows

$$\begin{aligned}
F = {} & \frac{\exp(i\omega t)}{4}\begin{pmatrix} \exp(2\eta\sqrt{g(b_2+i\omega)t}) \\ erfc\left(\eta\sqrt{g}+\sqrt{(b_2+i\omega)t}\right) \\ +\exp(-2\eta\sqrt{g(b_2+i\omega)t}) \\ erfc\left(\eta\sqrt{g}-\sqrt{(b_2+i\omega)t}\right)\end{pmatrix} \\
& + \frac{\exp(-i\omega t)}{4}\begin{pmatrix} \exp(2\eta\sqrt{g(b_2-i\omega)t}) \\ erfc\left(\eta\sqrt{g}+\sqrt{(b_2-i\omega)t}\right) \\ +\exp(-2\eta\sqrt{g(b_2-i\omega)t}) \\ erfc\left(\eta\sqrt{g}-\sqrt{(b_2-i\omega)t}\right)\end{pmatrix} \\
& + \frac{c}{2d}\begin{pmatrix} \exp\left(2\eta\sqrt{gb_2t}\right)erfc\left(\eta\sqrt{g}+\sqrt{b_2t}\right) \\ +\exp\left(-2\eta\sqrt{gb_2t}\right)erfc\left(\eta\sqrt{g}-\sqrt{b_2t}\right)\end{pmatrix} \\
& - \frac{c.\exp(dt)}{2d}\begin{pmatrix} \exp\left(2\eta\sqrt{g(b_2+d)t}\right) \\ erfc\left(\eta\sqrt{g}+\sqrt{(b_2+d)t}\right) \\ +\exp\left(-2\eta\sqrt{g(b_2+d)t}\right) \\ erfc\left(\eta\sqrt{g}-\sqrt{(b_2+d)t}\right)\end{pmatrix} \\
& - \frac{c}{2d}\begin{pmatrix} \exp\left(2\eta\sqrt{abt}\right)erfc\left(\eta\sqrt{a}+\sqrt{bt}\right)+ \\ \exp\left(-2\eta\sqrt{abt}\right)erfc\left(\eta\sqrt{a}-\sqrt{bt}\right)\end{pmatrix} \\
& + \frac{c\exp(dt)}{2d}\begin{pmatrix} \exp(2\eta\sqrt{a(b+d)t})\,erfc \\ \left(\eta\sqrt{a}+\sqrt{(b+d)t}\right) \\ +\exp(-2\eta\sqrt{a(b+d)t}) \\ erfc\left(\eta\sqrt{a}-\sqrt{(b+d)t}\right)\end{pmatrix}
\end{aligned} \tag{17}$$

$$\theta = \frac{1}{2}\begin{pmatrix} \exp(2\eta\sqrt{abt})\,erfc\left(\eta\sqrt{a}+\sqrt{bt}\right) \\ +\exp(-2\eta\sqrt{abt})\,erfc\left(\eta\sqrt{a}-\sqrt{bt}\right)\end{pmatrix} \tag{18}$$

where $a = \frac{L_5\,\mathrm{Pr}}{L_6}$, $b = \frac{R}{L_5\,\mathrm{Pr}}$, $b_1 = \frac{(1+im)M^2}{1+m^2}$,

$b_2 = \frac{L_4 b_1}{L_1}$, $c = \frac{L_2 Gr}{L_1 - L_3 a}$, $d = \frac{L_3 ab - L_4 b_1}{L_1 - L_3 a}$

Dharmaiah G et.al. [26] calculated and tabulated the skin friction coefficient, Nusselt number. The dimensionless skin friction coefficient, rate of heat transfer are given as follows

$$C_f = -\left(\frac{\partial F}{\partial z}\right)_{z=0} \tag{19}$$

$$Nu = -\left(\frac{\partial \theta}{\partial Z}\right)_{Z=0} \tag{20}$$

The velocity F has computed and represented by Eq. (17). Using the below formula, the complex error function is detached from real (U) and imaginary (V) parts separately. Real and imaginary parts are differentiated with initial conditions for calculating the Nusselt and Skin friction coefficient.

$$erf(a+ib) = erf(a) + \frac{\exp(-a^2)}{2a\pi}\left[1-\cos(2ab)+i\sin(2ab)\right]$$

$$+\frac{\exp(-a^2)}{\pi}\sum_{n=1}^{\infty}\frac{\exp\left(\frac{-n^2}{4}\right)}{n^2+4a^2}\left[f_n(a,b)+ig_n(a,b)\right]+\epsilon(a,b)$$

Where $f_n = 2a - 2a\cosh(nb)\cos(2ab) + n\sinh(nb)\sin(2ab)$

$g_n = 2a\cosh(nb)\sin(2ab) + n\sinh(nb)\cos(2ab)$

$\left|\epsilon(a,b)\right| \approx 10^{-16}\left|erf(a+ib)\right|$

RESULTS AND DISCUSSION

The primary velocity (U), the secondary velocity (V) are taken in terms of parameters M, Gr, t, Pr, ω, η, m, R. The numerical calculations of respective equations are computed and represented in several graphs. The primary and secondary velocity profiles of Alumina – Water with coordinate is represented by the graph from Figure 2 to Figure 17.

Effects of Different Parameters on The Primary and Secondary Velocity Profile.

The primary velocity U decreases with an increasing value of **t** is shown in Figure 2, if ❐ =π, φ=0.15, Pr=0.71,

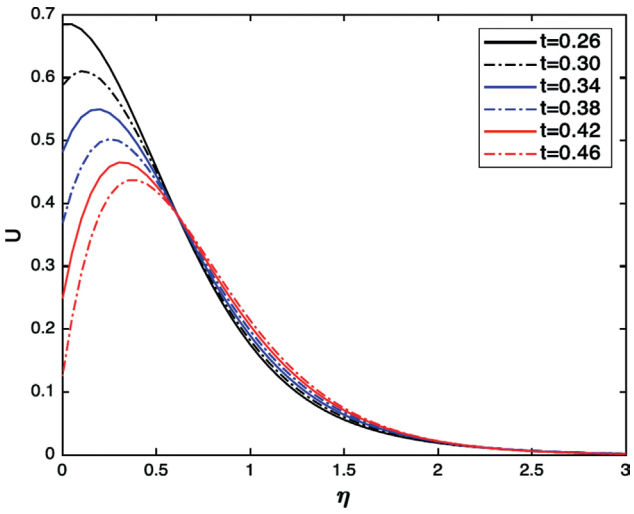

Figure 2. Primary velocity profile for various t.

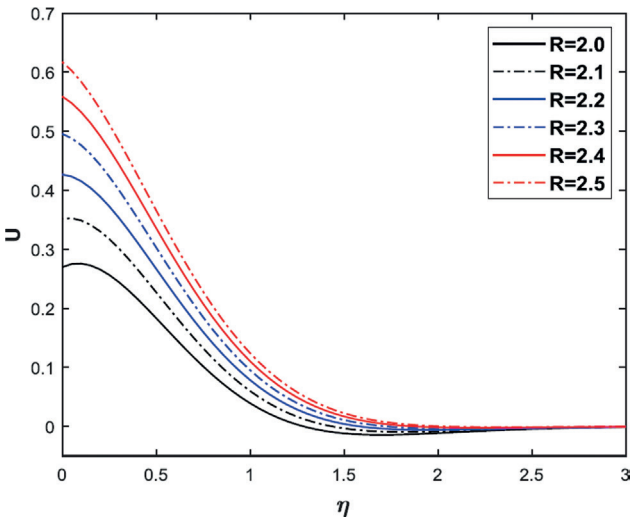

Figure 3. Primary velocity profile for various R.

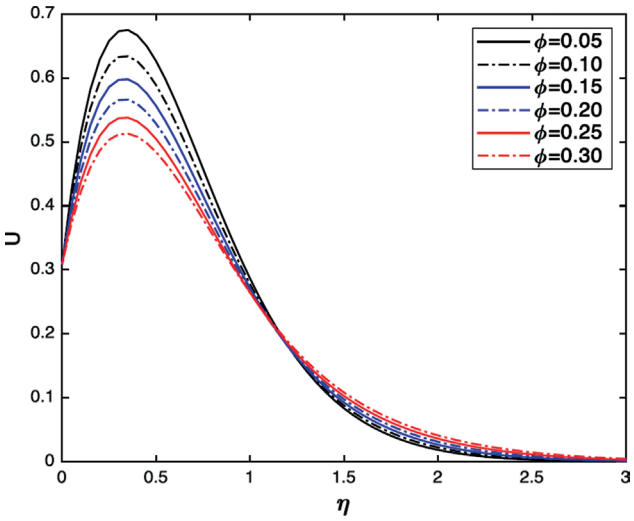

Figure 4. Primary velocity profile for various φ.

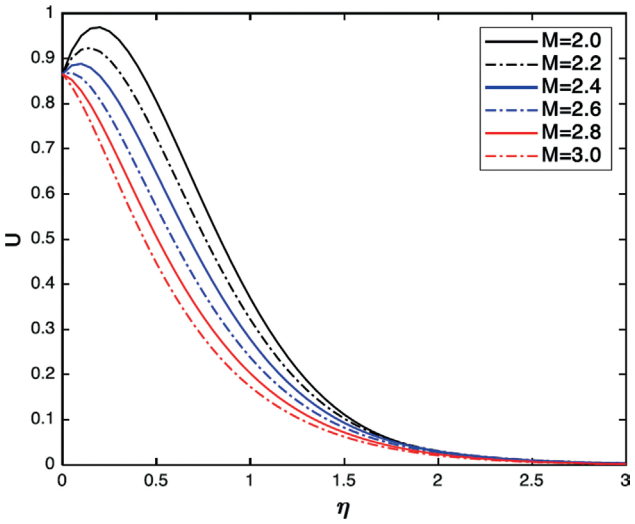

Figure 5. Primary velocity profile for a various M.

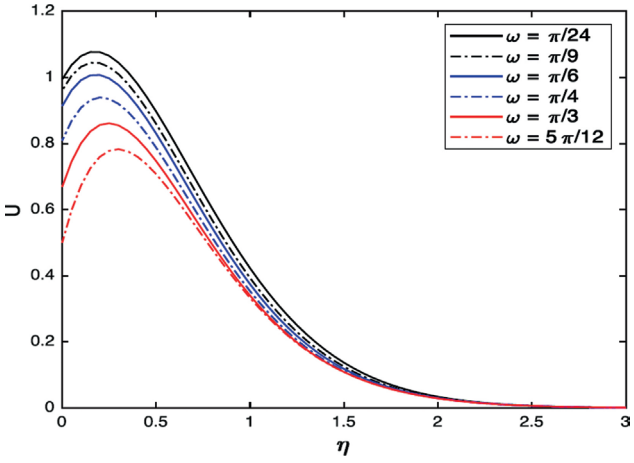

Figure 6. Primary velocity profile for various ω.

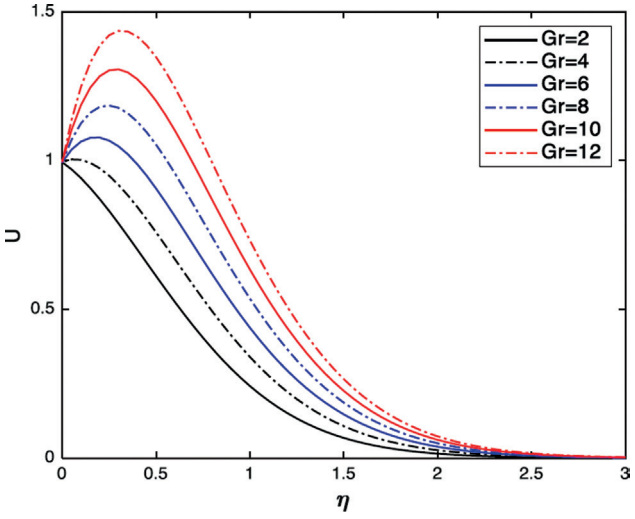

Figure 7. Primary velocity profile for various Gr.

R=0.5, t=0.26 to 0.46, Gr=3, M=1, m=1.it is observed that the secondary velocity V decreases with an increasing value of time (t) in Figure 11.

The primary velocity U and secondary velocity V increase with an increasing value of radiation (R) are illustrated in Figure 3 and Figure 16. The radiation increases the speediness of the fluid over the boundary layer field. The increment of solid volume fraction φ decreases the primary velocity U and secondary velocity V in Figure 4 and Figure 17. The density of fluid increases when nanoparticles are added to the base fluid and the fluid transforms into denser. It decreases the velocity of the fluid.

In Figure 5 and Figure 15, it is noted an increase in the magnetic field parameter (M) leads to a decrease in the primary velocity U and secondary velocity V. Due to the transverse magnetic field, Lorentz force is raised with a higher M value. It has a trend to slow down fluid motion. So both velocity is decreased with increasing values of magnetic field parameter. Baby rani et al. [27] explained Lorentz force who was resisted nanofluid flow and reduced the velocity.

In Figure 6, the phase angle ❒ increment from π/24 to 5π/12 reduced the primary velocity U. It is also noticed that the increase of phase angle has reduced the secondary velocity V in Figure 10. The velocity attains maximum

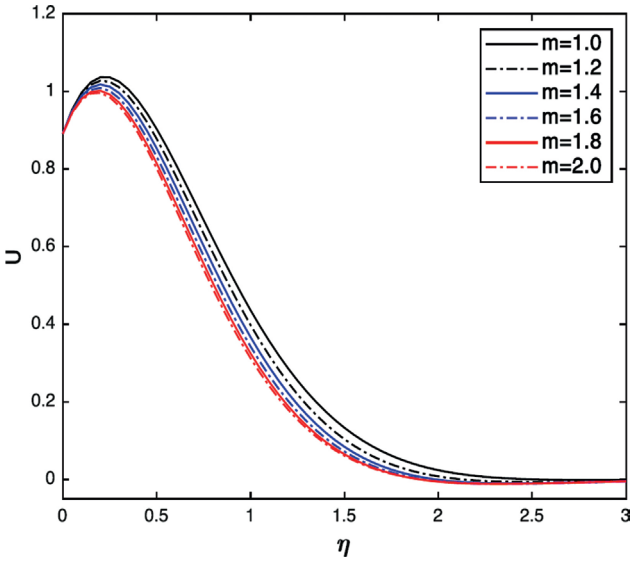

Figure 8. Primary velocity profile for various m.

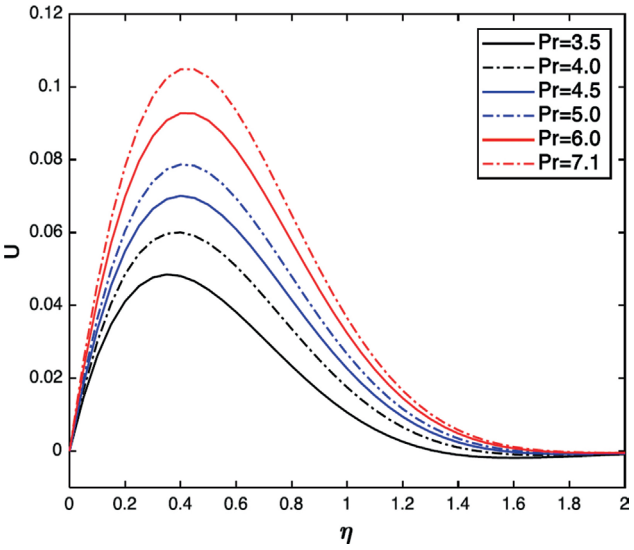

Figure 9. Primary velocity profile for various Pr.

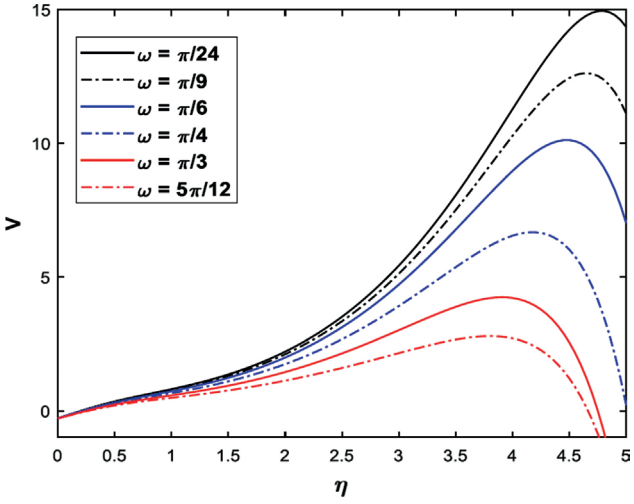

Figure 10. Secondary velocity profile for various ω.

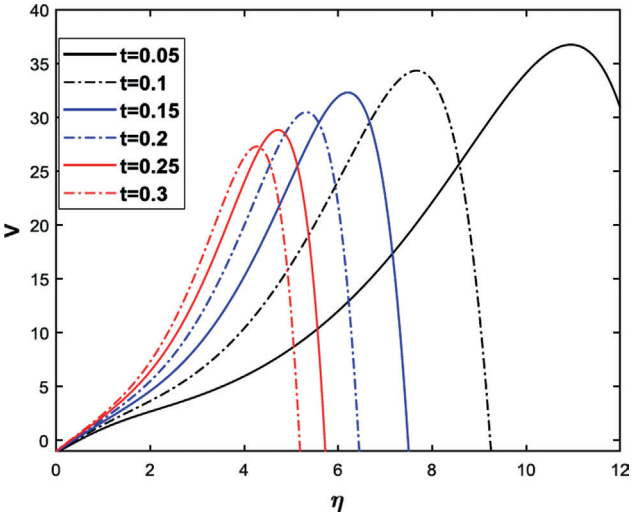

Figure 11. Secondary velocity profile for various t.

value if it is near a plate and the velocity decreasing with an increasing angle from the plate, finally approaches zero as z→ ∞.

The primary velocity U and secondary velocity V increase with an increasing value of Grashof number (Gr) are shown in Figure 7 and Figure 13. Gr is the ratio of the thermal buoyancy and viscous force that controls a fluid. The various values of Gr contribute to increasing the buoyancy force as well as decreasing the viscous forces. The fluid velocity will increase because the viscosity decreases as well as the internal resistance of the fluid decrease. In natural convection flow, the Grashof number increases the control of the flow. In the non-appearance of the free convection, the Grashof number is zero. In the cooling problem, the Grashof number has carried positive values. The cooling procedure is based on the Grashof number which is applied in the cooling of electronic components and nuclear reactors.

In Figure 8 and Figure 14, an increment of Hall parameter (m) value had reduced in Primary velocity U and secondary velocity V. Both velocity profiles decreased if m values are large, $\frac{M^2}{(1+m^2)}$ became very small then the magnetic field diminishes. An increase in *m* decreases whose active conductivity leads to magnetic restraining.

The primary velocity U and secondary velocity V increase with an increasing value of Prandtl number (Pr) are represented in Figure 9 and Figure 12. An increment

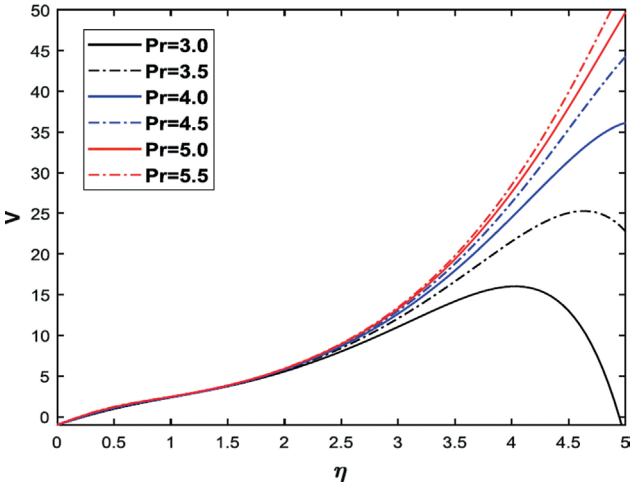

Figure 12. Secondary velocity profile for various Pr.

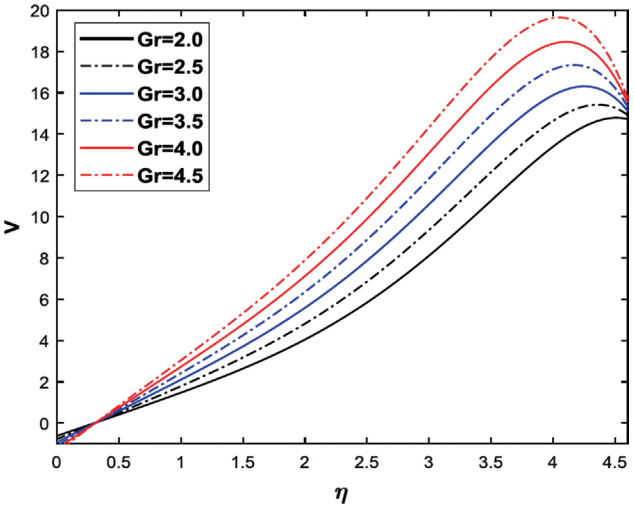

Figure 13. Secondary velocity profile for various Gr.

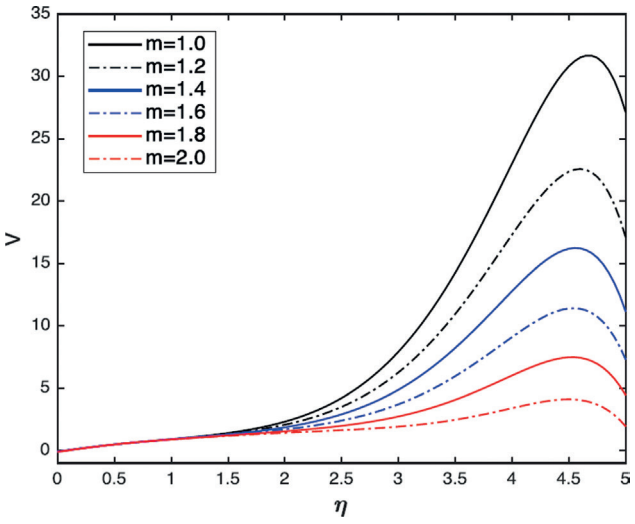

Figure 14. Secondary velocity profile for various m.

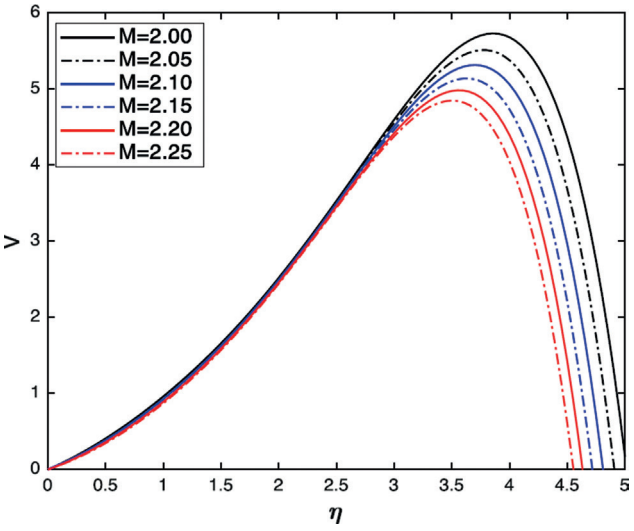

Figure 15. Secondary velocity profile for various M.

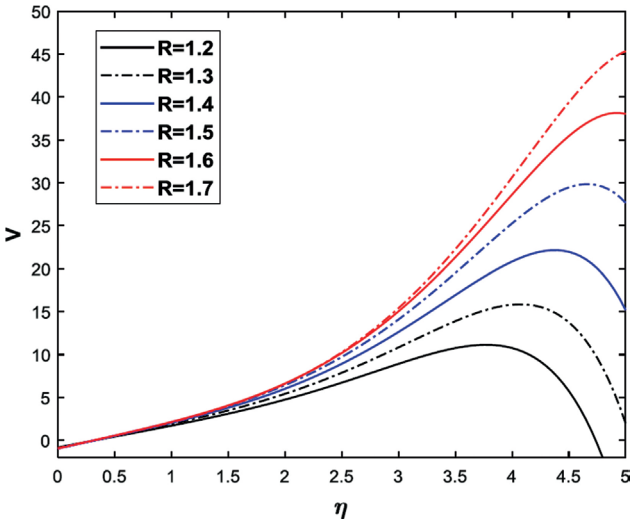

Figure 16. Secondary velocity profile for various R.

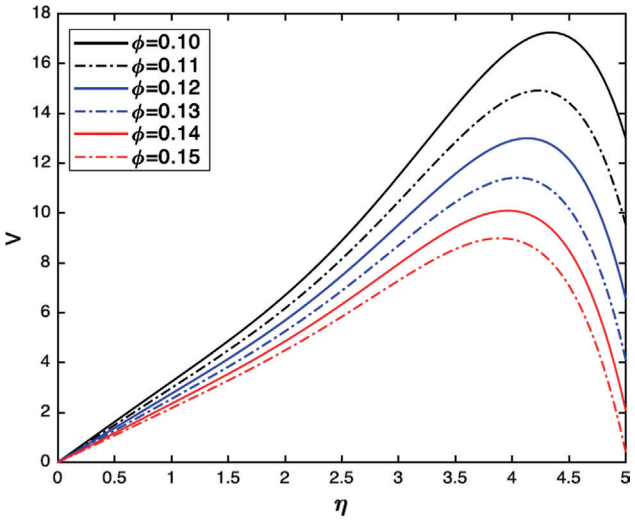

Figure 17. Secondary velocity profile for various φ

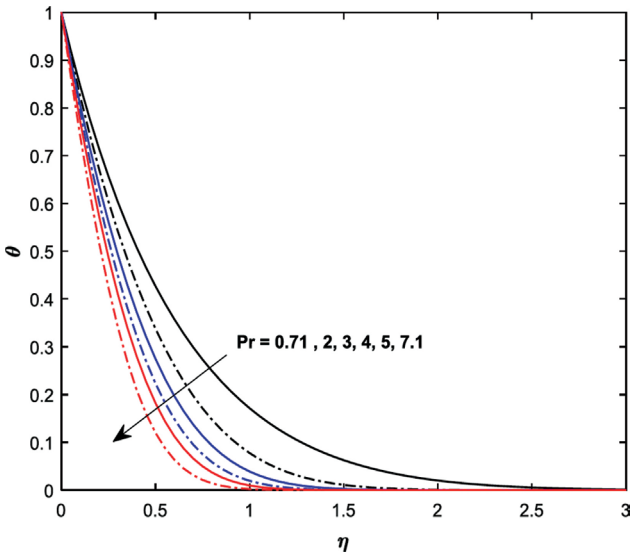

Figure 18. Temperature profile for different Pr**.**

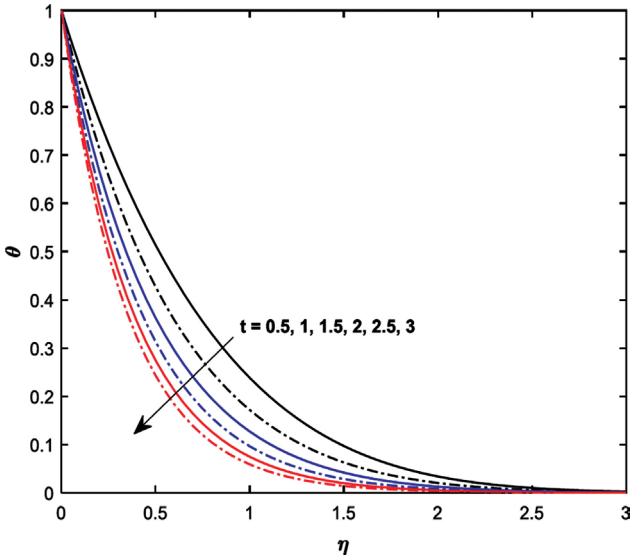

Figure 19. Temperature profile for different t.

of Prandtl number increase the Primary velocity U and secondary velocity V.Due to the Prandtl number increase, boundary layer thickness increases.it leads to an increase in the velocities.

Effects of Parameters on Temperature Profiles

The heat transfer rate is existed high in air comparing with water by Muthucumaraswamy et al. [2]. So temperature increases while decreasing the Prandtl number. The ratio of viscosity to thermal diffusivity is called the Prandtl number. An increase in thermal diffusivity points to a decrease in the Prandtl number. Thermal diffusion has a propensity to reduce the fluid temperature. The temperature profile for different values of Pr has presented in Figure 18. The temperature profile for different values of t has presented in Figure 19. It has been found that the temperature of Alumina-water nanofluid decreased with increasing values of time t.

The temperature profiles for different values of radiation parameter and solid volume fraction have shown in Figure 20. and Figure 21. It has been generated that the temperature of Alumina– Water nanofluid decreases with

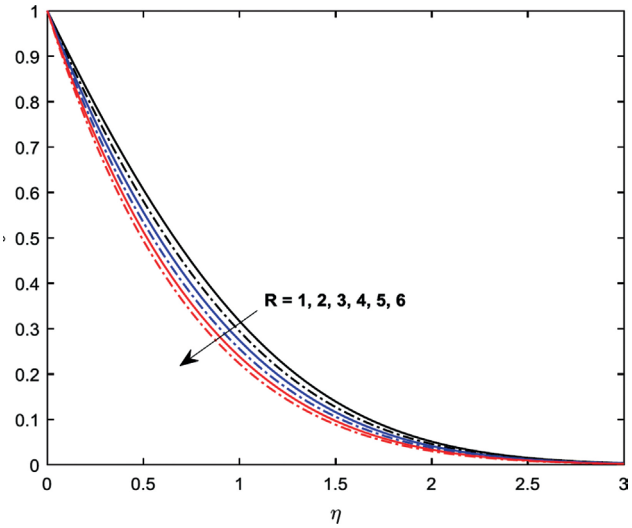

Figure 20. Temperature profile for different R.

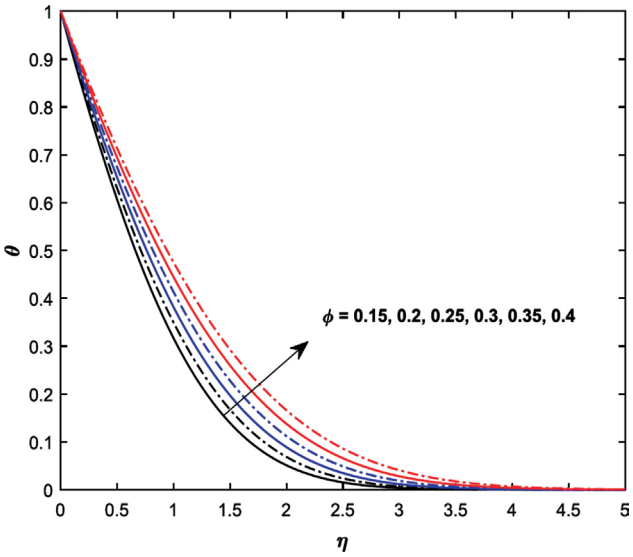

Figure 21. Temperature profile for different ☐

Table 2. Variations in Nusselt Number

t	Pr	☐	R	$-\theta'(0)$
0.5	0.71	0.15	1	1.2583
0.6	0.71	0.15	1	1.3459
0.7	0.71	0.15	1	1.4302
1.0	**0.71**	0.15	1	1.6657
1.0	**2.00**	0.15	1	1.8879
1.0	**3.00**	0.15	1	2.0754
0.1	0.71	**0.15**	1	0.8688
0.1	0.71	**0.20**	1	0.8102
0.1	0.71	**0.25**	1	0.7560
0.3	0.71	0.15	**2**	1.3459
0.3	0.71	0.15	**3**	1.5899
0.3	0.71	0.15	**4**	1.8101

Table 3. Comparison of the values of Nusselt number

☐	Ref.[5]	Present Study
0.02	1.9334	1.0492
0.04	1.7238	1.0182
0.06	1.5333	0.9885
0.08	1.3603	0.9601

increasing values of R. The temperature profile for different values of φ has displayed in Figure 21. It has been found that the temperature of Alumina-water nanofluid increases with increasing values of solid volume fraction φ.

Effects of Parameters of Skin Friction Coefficient and Nusselt Number

Friction is played a major role in a lot of engineering fields such as transportation, household usage, and measurements. Skin friction is a component of drag, the force resisting the motion of a fluid across the surface of a body. Veerakrishna et.al. [12] had calculated and listed skin friction coefficient, Nusselt number, and Sherwood number. He also revealed that skin friction increased due to an increase of urge by force and it diminished with the rise in magnetic parameter M, phase angles ω, and Grashof number. The particle size $\varphi = 0.15$ has been taken for Nusselt number and skin friction coefficient exploration.The numerical effects of solid volume fraction, radiation parameter, Prandtl number with various times on heat transfer coefficients are calculated and listed in Table.2.

From Table 2, the.Nusselt number values are gradually increased with increasing time t and t radiation R.

If Pr=0.71, Pr=2, Pr=3 then the Nusselt number values are increasing. Since free and forced convection, the Prandtl Number usage is high for heat transfer calculation with fluidproperties. In heat transfer, the Nusselt number is calculated to identify the heat transfer which is conduction or convection. The Nusselt number values of various solid volume fractions (☐) in the reference paper and the present study are shown in Table 3 which is decreasing with the increased values of particle size. In Figure 22, the Nusselt number increases with the increment of radiation

In Figure 23, Skin friction values are increased with increasing values of Hall parameter (m). The MHD flow

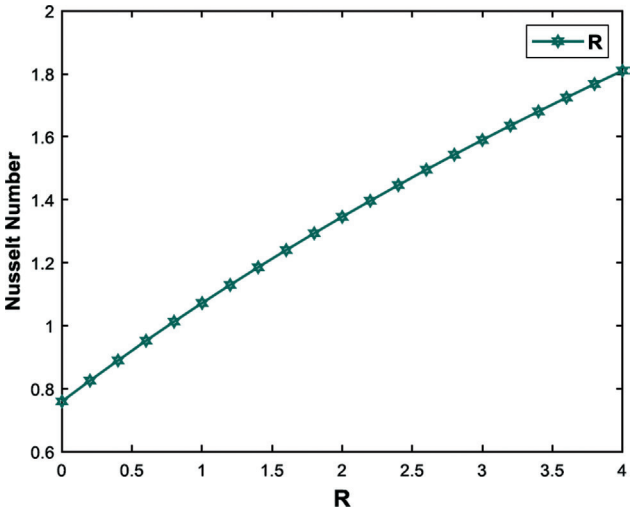

Figure 22. Nusselt number for different values of R.

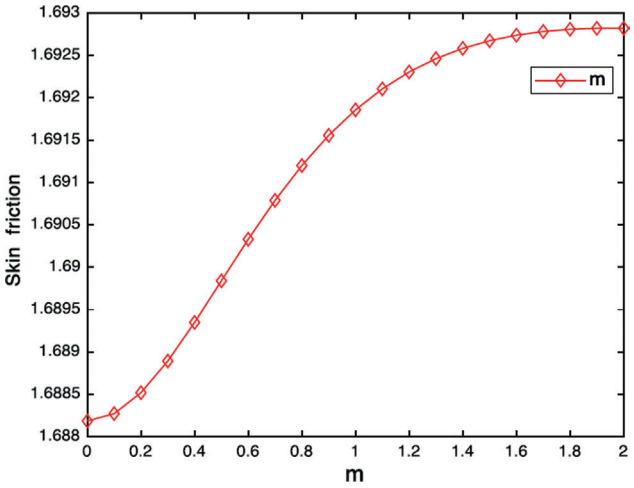

Figure 23. Skin friction coefficient for different values of m.

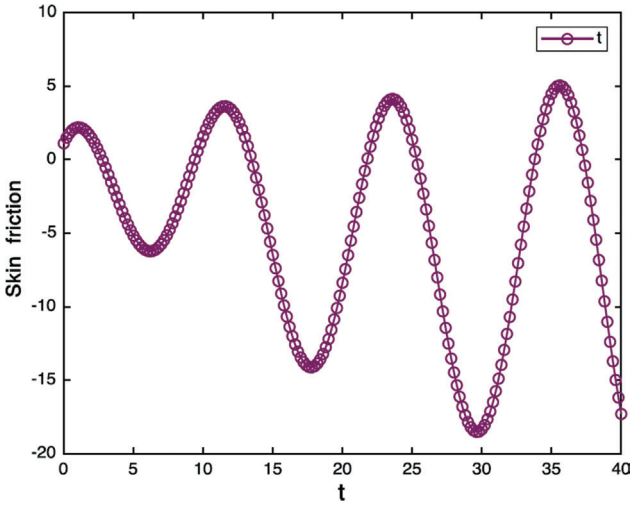

Figure 24. Skin friction coefficient values for different t in U.

with Hall current is used in the flight synchrotron. From Figure 24 and Figure 25, the Skin friction coefficient has either increased or decreased with a different time in Primary and secondary velocity. The skin friction values are compared with parameter radiation in Table 4.

The time (t), Prandtl number (Pr), Grashof number (Gr), Hall parameter (m), Magnetic parameter (M), radiation (R), phase angle (ω) parameters are considered to calculate skin friction coefficient values. It is listed in Table 5 and Table 6.

Table 4. Comparison of the values of skin friction coefficient (C_f)

R	Ref [26]	Present Study
0.02	0.8887	-0.0476
0.04	0.9032	-0.0390
0.06	0.9096	-0.0306

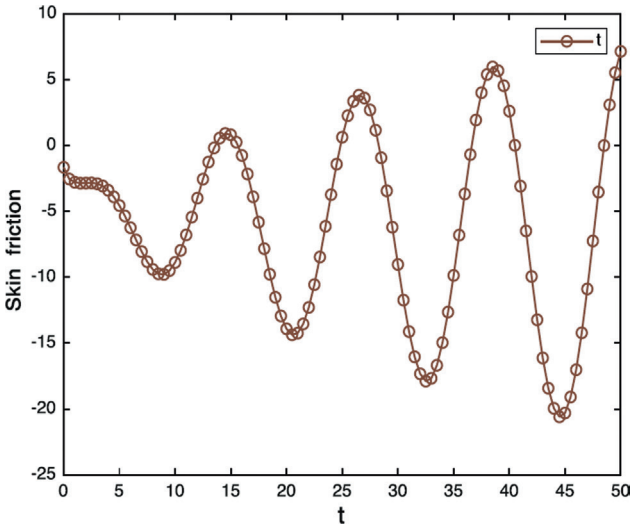

Figure 25. Skin friction coefficient values for different t in V.

CONCLUSION

The main exertion of the paper is to acquire the exact solution and to find the influence of Heat transfer and Hall Effects for the unsteady free convective Aluminananofluid flow over an oscillating plate with the existence of thermal radiation and magnetohydrodynamic. The primary and secondary velocity and temperature existence explained.

Table 5. Variations in Skin friction coefficient values of Primary Velocity (U)

t	Pr	R	m	M	Gr	❐	C_f
0.2	4.0	1.0	0.1	1.0	2.0	π/6	1.4930
0.4							1.7912
0.6							2.0058
3.6							–2.0344
3.8							–2.5403
4.0							–3.0382
0.2	**1.0**	1.0	0.6	1.0	3.0	π/3	0.8295
	1.5						0.8682
	2.0						1.5645
1	0.71	**2.0**	0.5	2	5.0	π/4	0.4745
		2.2					0.5054
		2.4					0.5344
0.2	3.0	1.2	**0.2**	0.2	4.0	π/6	1.6885
			0.3				1.6889
			0.4				1.6893
0.6	0.71	0.2	0.5	**2.0**	5.0	π/5	2.5994
				4.0			7.0455
				15.0			29.3983
0.3	2.0	0.9	0.6	1.0	**3.0**	π/7	1.6886
					11.0		2.5698
					20.0		3.5612
0.7	4.0	1.5	0.7	1.1	6.0	**π/8**	3.8620
						π/4	3.5230
						π/2	2.3037

In the probe of the oscillating plate and nanofluid flow, the highlights of concluding remarks have been summarized as followed.

- The velocity of fluid increases with the increasing values of radiation parameter, Prandtl parameter, Grashof number in both primary and secondary flows.
- The temperature of the fluid decreases with the increasing values of radiation parameter, time, and Prandtl parameter. But increasing solid volume leads to an increase the temperature.
- The Nusselt number values decrease with the increasing value of particle size.
- In primary velocity (U),the skin friction values are increased with increasing values of radiation, Hall parameter, Magnetic parameter, Prandtl number. In secondary velocity (V), the skin friction value is increased when M and ? are increased.

NOMENCLATURE

List of symbols

B_0 Constant applied magnetic field (Wbm-2)
C_p Specific heat at constant pressure (J kg^{-1} K^{-1})
C_f Coefficient of Skin Friction
E Electric field (kJ)
F Complex Function
g Gravity acceleration (ms^{-2})
Gr Thermal Grashof number
M Dimensionless magnetic field parameter
m Hall Parameter
Nu Nusselt Number
n Dimensionless frequency
Pr Prandtl number
$\bar{q_w}$ Dimensional heat flux from the plate
t^* Time(s)
t Dimensionless time (s)

Table 6. Variations in Skin friction coefficient values of secondary velocity (V).

t	Pr	R	m	M	Gr	❐	C_f
0.4	4.0	1.0	0.1	1.0	2.0	π/6	-2.2325
0.8							-2.7262
1.2							-2.8376
37.0							1.9283
37..5							4.0061
38.0							5.3854
0.2	**0.91**	1.0	0.6	1.0	3.0	π/3	-3.3957
	5.1						-7.7970
	6.5						-8.7319
1	0.71	**1**	0.5	2	5.0	π/4	0.6763
		2					0.1916
		3					-0.5366
0.2	3.0	1.5	**0.7**	2.2	4.0	π/6	-0.3228
			1.4				-0.4603
			2,1				-0.6365
0.6	0.71	0.2	0.5	**2.0**	5.0	π/5	0.4066
				17.0			5.4559
				23.0			7.3299
0.3	2.0	0.9	0.6	1.0	**9.00**	π/7	-15.1724
					27.0		-45.9262
					36.0		-61.3031
0.7	4.0	1.5	0.7	1.1	6.0	**π/8**	-12.4594
						π/4	-12.1251
						π/2	-11.5056

T Local temperature of the nanofluid (K)
T_w Wall temperature (K)
T_∞ The temperature of the ambient nanofluid (K)
$u^\star, v^\star, w^\star$ Velocity components along $x^\star$, $y^\star$, $z^\star$ axes
U, V, W Dimensionless velocity components
x, y, z Cartesian coordinates

Greek symbols
α Thermal diffusivity ($m^2 s^{-1}$)
β Thermal expansion coefficient (K^{-1})
ε Dimensionless small quantity (<<1)
φ Solid volume fraction of the nanoparticles
ρ Density
k Thermal conductivity ($m^2 s^{-1}$)
μ Dynamic viscosity (Pa s)
ϑ Kinematic viscosity ($m^2 s^{-1}$)
θ Dimensionless temperature
η Pseudo-similarity variable
ω Phase angle
σ Electrical conductivity ($m^2 s^{-1}$)

Superscript
– Dimensional quantities

Subscripts
f Fluid
nf Nanofluid
s Solid

AUTHORSHIP CONTRIBUTIONS

Authors equally contributed to this work.

DATA AVAILABILITY STATEMENT

The authors confirm that the data that supports the findings of this study are available within the article. Raw

data that support the finding of this study are available from the corresponding author, upon reasonable request.

CONFLICT OF INTEREST

The author declared no potential conflicts of interest with respect to the research, authorship, and/or publication of this article.

ETHICS

There are no ethical issues with the publication of this manuscript.

REFERENCES

[1] Nguyen CT, Roy G, Gauthier C, Galanis N. Heat transfer enhancement using Al2O3-water nanofluid for an electronic liquid cooling system. Appl Therm Eng 2007;27:1501–1506. [CrossRef]

[2] Muthucumaraswamy R, Lal T, Ranganayakulu D. Effects of rotation on MHD flow past an accelerated isothermal vertical plate with heat and mass diffusion. Theor Appl Mech 2010;37:189–202. [CrossRef]

[3] Sridhara V, Satapathy LN. Al_2O_3 -based nanofluids : A review. Sridhara Satapathy Nanoscale Res Lett 2011;6:1–16. [CrossRef]

[4] Sarkar BC, Das S, Jana RN. Effects of hall currents and radiation on MHD free convective flow past an oscillating vertical plate with oscillatory plate temperature in a porous medium. Bull Soc Math Serv Stand 2012;3:5–27. [CrossRef]

[5] Lee S, Choi S, Li S, Eastman J. Measuring thermal conductivity of fluids containing oxide nanoparticles. Heat Transf 2013;121:280–289. [CrossRef]

[6] Pal D, Talukdar B. Influence of hall current and thermal radiation on MHD convective heat and mass transfer in a rotating porous channel with chemical reaction. Int J Eng Math 2013;2013:1–13. [CrossRef]

[7] Reza Mohaghegh M. Numerical solution of linear and nonlinear periodic physical problems using fourier spectral method. J Comput Sci Comput Math 2013;3:39–48. [CrossRef]

[8] Roy S, Asirvatham LG, Kunhappan D, Cephas E, Wongwises S. Heat transfer performance of Silver/Water nanofluid in a solar flat-plate collector. J Therm Eng 2015;1:104–112. [CrossRef]

[9] Rajesh V, Mallesh MP, Sridevi C. Transient MHD nanofluid flow and heat transfer due to a moving vertical plate with thermal radiation and temperature oscillation effects. Procedia Eng 2015;127:901–908. [CrossRef]

[10] Mohaghegh MR, Rahimi AB. Three-dimensional stagnation-point flow and heat transfer of a dusty fluid toward a stretching Sheet. J Heat Transfer 2016;138:1–12. [CrossRef]

[11] Das S, Jana RN, Makinde OD. The magnetohydrodynamic free convective flow of nanofluids past an oscillating porous flat plate in a rotating system with thermal radiation and hall effects. J Mech 2016;32:197–210. [CrossRef]

[12] Krishna MV, Reddy MG. MHD Convective rotating flow past an oscillating porous plate with chemical reaction and Hall effects. IOP Conf Ser Mater Sci Eng 2016;149:012217. [CrossRef]

[13] Babu DD, Venkateswarlu S, Reddy EK. Heat and mass transfer on unsteady MHD free convection rotating flow through a porous medium over an infinite vertical plate with hall effects. AIP Conf Proc 2017;1859:87–103. [CrossRef]

[14] Obulesu M, Sivaprasad R. Hall current effects on MHD Convective flow past a porous plate with thermal radiation, chemical reaction and heat generation /absorption. Phys J 2019;2:104–125. [CrossRef]

[15] Hussain SM, Jain J, Seth GS, Rashidi MM. Free convective heat transfer with hall effects, heat absorption, and chemical reaction over an accelerated moving plate in a rotating system. J Magn Magn Mater 2017;422:112–123. [CrossRef]

[16] Seth GS, Bhattacharyya A, Tripathi R. Effect of hall current on MHD natural convection heat and mass transfer flow of rotating fluid past a vertical plate with ramped wall temperature. Front Heat Mass Transf 2017;9:1–12. [CrossRef]

[17] Yildiz S. Investigation of natural convection heat transfer at constant heat flux along with a vertical and inclined plate. J Therm Eng 2018;4:2432–2444. [CrossRef]

[18] Kataria HR, Patel HR. Heat and mass transfer in magnetohydrodynamic (MHD) Casson fluid flow past over an oscillating vertical plate embedded in a porous medium with ramped wall temperature. Propuls Power Res 2018;7:257–267. [CrossRef]

[19] Vijayalakshmi K, Umadevi R, Muthucumaraswamy R. Oscillating plate in nanofluid with uniform heat and mass flux under the effect of MHD, radiation, and chemical reaction is analyzed by Runge-Kutta method. TAGA J 2018;14:793–803. [CrossRef]

[20] Iqbal Z, Akbar NS, Azhar E, Maraj EN. Performance of hybrid nanofluid (Cu-CuO/water) on MHD rotating transport in oscillating vertical channel inspired by Hall current and thermal radiation. Alexandria Eng J 2018;57:1943–1954. [CrossRef]

[21] Arifuzzaman SM, Khan MS, Mehedi MFU, Rana BMJ, Ahmmed SF. Chemically reactive and naturally convective high-speed MHD fluid flow through an oscillatory vertical porous plate with heat and radiation absorption effect. Eng Sci Technol Int J 2018;21:215–228. [CrossRef]

[22] Sheri SR, Thumma T. Numerical study of heat transfer enhancement in MHD free convection flow over vertical plate utilizing nanofluids. Ain Shams Eng J 2018;9:1169–1180. [CrossRef]

[23] Radha Madhavi M, Nalleboyina V, Nagesh P. Influence of magnetic field, heat radiation and external surface temperature on nanofluids with different base fluids in mixed convective flows over a vertical circular cylinder. Int J Innov Technol Explor Eng 2019;8:497–504.

[24] Khan A, Khan D, Khan I, Ali F, Ul Karim F, Nisar KS. MHD flow of Brinkman type H2O-Cu, Ag, TiO2, and Al2O3 nanofluids with chemical reaction and heat generation effects in a porous medium. J Magn 2019;24:262–270. [CrossRef]

[25] Patel HR. Effects of heat generation, thermal radiation, and hall current on MHD Casson fluid flow past an oscillating plate in a porous medium. Multiph Sci Technol 2019;31:87–107. [CrossRef]

[26] Dharmaiah G, Sridhar W, Balamurugan KS, Chandra Kala K. Hall and ion slip impact on magneto-titanium alloy nanoliquid with diffusion thermo and radiation absorption. Int J Ambient Energy 2022;43:3507–3517. [CrossRef]

[27] Baby Rani CH, Vedavathi N, Balamurugan KS, Dharmaiah G. Hall and ion slip effects on ag-water based MHD nanofluid flow over a semi-infinite vertical plate embedded in a porous medium. Front Heat Mass Transf 2020;14:1–11. [CrossRef]

[28] Manjula V, Sekhar KVC. Effects of hall current, Dufour on unsteady MHD chemically reacting Casson fluid flow over an inclined oscillating plate with thermal radiation. Int J Sci Technol Res 2020;9:6439–6452.

[29] Balaji T, Selvam C, Mohan Lal D. A review on electronics cooling using nanofluids. IOP Conference Series: Materials Science and Engineering, International Conference on Advances in Renewable and Sustainable Energy Systems (ICARSES 2020) 3rd-5th December, Chennai, India. 2020;1130:012007. [CrossRef]